Accepted author's manuscript. Published in final edited form as: JACC Cardiovascular Imaging 2020 (in press). Publisher DOI: 10.1016/j.jcmg.2020.02.028

Shear stress estimated by quantitative coronary angiography predicts plaques prone to progress and cause events

Short title: 3D-QCA modelling and vulnerable plaque detection

Christos V. Bourantas,[a,b,c,#,*] MD, PhD; Thomas Zanchin,[a,d,e,#] MD; Ryo Torii,[e] PhD; Patrick W. Serruys,[f] MD, PhD; Alexios Karagiannis,[g] PhD; Anantharaman Ramasamy,[a,c] MBChB, MRCP; Hannah, Safi,[b] PhD; Ahmet Umit Coskun,[h] PhD; Gerhard Koning,[i] MSc; Yoshinobu Onuma,[j] MD, PhD; Christian Zanchin,[d] MD; Rob Krams,[k] MD, PhD; Anthony Mathur,[a,c] MD, PhD; Andreas Baumbach,[a,c] MD, FRCP; Gary Mintz,[l] MD; Stephan Windecker,[d] MD; Alexandra Lansky,[b,m] MD; Akiko Maehara,[l] MD; Peter H. Stone,[n] MD; Lorenz Raber,[d] MD, PhD; Gregg W. Stone,[m] MD

[a] Department of Cardiology, Barts Heart Centre, Barts Health NHS, London, UK
[b] Institute of Cardiovascular Sciences, University College London, London, UK
[c] Centre for Cardiovascular Medicine and Device Innovation, Queen Mary University London, London, UK
[d] Department of Cardiology, Bern University Hospital, Bern, Switzerland
[e] Department of Mechanical Engineering, University College London, London, UK
[f] Faculty of Medicine, National Heart & Lung Institute, Imperial College London, UK
[g] CTU Bern, Institute of Social and Preventive Medicine, Bern University, Bern, Switzerland
[h] Mechanical and Industrial Engineering, Northeastern University, Boston, MA
[i] Medis medical imaging systems bv, Leiden, The Netherlands
[j] Department of Interventional Cardiology, Thoraxcenter, Erasmus Medical Center, Rotterdam, the Netherlands
[k] Department of Molecular Bioengineering Engineering and Material Sciences, Queen Mary University London, London, UK
[l] Department of Cardiology, Columbia University Medical Center and the Cardiovascular Research Foundation, New York, NY
[m] Division of Cardiovascular Medicine, Department of Internal Medicine, Yale School of Medicine, New Haven, CT
[n] Cardiovascular Division, Brigham & Women's Hospital, Harvard Medical School, Boston, MA

[#] The first two authors have contributed equally to the preparation of this manuscript

***Address for correspondence**
Dr Christos Bourantas, MD, PhD
Consultant Cardiologist,
Barts Heart Centre
West Smithfield, London EC1A 7BE, UK
E-mail: cbourantas@gmail.com
Phone: +44 20 7377 7000
Fax: +44 20 7791 9670

Funding: Thomas Zanchin is supported by the Swiss National Science Foundation grant number 323530-171146.
Hannah Safi is founded by British Heart Foundation (PG/17/18/32883) while Anantharaman Ramasamy, Anthony Mathur, Andreas Baumbach and Christos V. Bourantas by Barts Biomedical Research Centre.

Conflict of interest: Prof Serruys, Prof Stone and Dr Maehara have received personal fees from Philips/Volcano and Abbott Vascular, Dr Bourantas from Philips/Volcano, Mr Koning from Medis Medical Imaging Systems, and Prof Raber and Windecker have received grants from Abbott. None of the other authors have a conflict of interest to declare.

Abstract

Objectives: To examine the value of endothelial shear stress (ESS) estimated in three-dimensional quantitative coronary angiography (3D-QCA) models in detecting plaques that are likely to progress and cause events.
Background: Cumulative evidence have shown that plaque characteristics and the ESS derived from intravascular ultrasound (IVUS)-based reconstructions enable prediction of lesions that will cause cardiovascular events. However, the prognostic value of the ESS estimated by 3D-QCA in non-flow limiting lesions is yet unclear.
Methods: We analysed the baseline virtual histology (VH)-IVUS and angiographic data from 28 lipid-rich lesions (i.e., fibroatheromas) that caused major adverse cardiovascular events or required revascularization (MACE-R) at 5-year follow-up and from a control group of 119 lipid-rich plaques that remained quiescent. The segments studied by VH-IVUS at baseline were reconstructed using 3D-QCA software and in the obtained geometries blood flow simulation was performed and we estimated the pressure gradient across the lipid-rich plaque and the mean ESS values in 3mm segments. The additive value of these hemodynamic indices in predicting MACE-R beyond plaque characteristics was examined.
Results: MACE-R lesions were longer, had smaller minimum lumen area (MLA), increased plaque burden (PB), were exposed to higher ESS, and exhibited a higher pressure gradient. In multivariable analysis plaque burden (hazard ratio: 1.08, P=0.004) and the maximum 3mm ESS value (hazard ratio: 1.11, P=0.001) were independent predictors of MACE-R. Lesions exposed to high ESS (>4.95Pa) with a high-risk anatomy (MLA<4mm^2 and PB>70%) had a higher MACE-R rate (53.8%) than those with a low-risk anatomy exposed to high ESS (31.6%) or those exposed to low ESS that had high (20.0%) or low-risk anatomy (7.1%, P<0.001).
Conclusions: In the present study, 3D-QCA-derived local hemodynamic variables provided useful prognostic information and in combination with lesion anatomy enabled more accurate identification of MACE-R lesions.

Keywords: Vulnerable plaque; quantitative coronary angiography; shear stress.

Abbreviations:

3D:	three dimension
DS:	diameter stenosis
EEM:	external elastic membrane
ESS:	endothelial shear stress
MACE-R:	major adverse cardiovascular events – revascularisation
MLA:	minimum lumen area
MLD:	minimum lumen diameter
QCA:	quantitative coronary angiography
PB:	plaque burden
TCFA:	thin cap fibroatheroma
ThCFA:	thick cap fibroatheroma
VH-IVUS:	virtual histology intravascular ultrasound

Introduction

Prospective invasive imaging studies of coronary atherosclerosis have provided robust evidence that intravascular imaging can identify, although with only modest accuracy, vulnerable plaques that are likely to progress and cause cardiovascular events (1,2). Computational fluid dynamic analysis of models reconstructed by intravascular imaging data and estimation of the local hemodynamic forces appears to provide additional prognostic information, and recent reports have shown that when they are combined with plaque characteristics they enable accurate detection of lesions that will progress and cause events (3,4). However, intravascular imaging-based reconstruction and blood flow simulation processing is a tedious and time consuming process that requires dedicated software and expertise, thus limiting its use in everyday clinical practice.

Conversely, three dimensional quantitative coronary angiography (3D-QCA) can be performed in real-time while the patient is on the catheterization laboratory and appears able to accurately assess lumen dimensions and the extent and the severity of coronary artery disease. Recently, we have processed 3D-QCA models with computational fluid dynamic techniques and demonstrated that the estimated endothelial shear stress (ESS) was predictor of atherosclerotic disease progression at 1-year follow-up; in addition a post-hoc analysis of the FAME (Fractional Flow Reserve versus Angiography for Multivessel Evaluation) II study showed that the 3D-QCA-derived ESS estimated in hemodynamically severe stenoses predicted those that caused myocardial infarction at 3 years follow-up (5,6). However, the combined value of plaque characteristics and of the ESS estimated by 3D-QCA in non-flow limiting plaques in predicting these that are likely to progress and cause events is yet unclear.

Methods

Studied patients

The present study is a post hoc analysis of data acquired in the PROSPECT (Providing Regional Observations to Study Predictors of Events in the Coronary Tree) and IBIS 4 (Intergraded Biomarkers Imaging Study-4) studies. The design of both studies, the inclusion and exclusion criteria and the endpoints and definitions have been described in detail elsewhere (2,7). In brief the PROSPECT was a large-scale prospective invasive imaging study that aimed to investigate the value of virtual histology intravascular ultrasound (VH-IVUS) imaging in detecting vulnerable plaques that will progress and cause events. The study included 697 patients admitted with an acute coronary syndrome that had successful percutaneous coronary intervention in all the culprit lesions and 3-vessel VH-IVUS imaging of the proximal 60-80mm segment. IBIS 4 study was a multicentre multimodality imaging study that aimed to examine the effect of aggressive statin therapy (rosuvastatin 40mg once daily) on plaque burden and composition in patients admitted with ST-elevation myocardial infarction. All the recruited patients (n=103) had successful revascularization and 3-vessel VH-IVUS and optical coherence tomography imaging of the proximal 50mm segment at baseline and 13-month follow-up. The patients recruited in the PROSPECT study were followed-up for a median of 3.4 years while those recruited in the IBIS 4 for 5 years.
Both studies complied with the Declaration of Helsinki and were approved by the ethics committees of all the participant centres.

Clinical endpoints

The primary endpoint of the PROSPECT study was the composite endpoint of cardiac death or arrest, myocardial infarction, or re-hospitalization for unstable or progressive angina. The IBIS 4 study had an imaging-based endpoint (i.e., the change in the percent atheroma volume at 13 months follow-up); however in that study – which was a sub-study of the COMFORTABLE-AMI study – clinical endpoints were also recorded including cardiac death, myocardial infarction and target and non-target lesion revascularization. In the IBIS 4

study revascularisation was deemed clinically indicated at follow-up angiography when there was a percent diameter stenosis (%DS) ≥70% on QCA or 70%≥%DS≥50% and recurrent angina or evidence of ischaemia at rest or during an exercise test.

The clinical, angiographic and intravascular imaging data in both studies enabled identification of the untreated lesions that were assessed by VH-IVUS at baseline and caused events. The present analysis focused on these lesions; the primary endpoint of this study is the combined endpoint of cardiac death, myocardial infarction, or revascularisation because of progressive or unstable angina, or because of evidence of ischemia and 70%≥%DS≥50% on follow-up coronary angiography or because of significant disease progression (%DS≥70%) at follow-up angiography (MACE-R). Secondary endpoint of the present analysis is the combined endpoint of cardiac death, myocardial infarction, or revascularisation because of progressive or unstable angina (MACE).

Studied lesions and VH-IVUS analysis

In the PROSPECT study 25 of the untreated lesions at baseline that were studied by VH-IVUS and caused events had a thin cap fibroatheroma phenotype (TCFA), 18 a thick cap fibroatheroma phenotype (ThCFA), 7 a non-fibroatheroma phenotype and 4 were unclassified lesions. In the IBIS 4 study all the lesions associated with MACE-R had either a TCFA (n=13) or a ThCFA (n=2) phenotype (2,4). The present analysis included only untreated lesions with a lipid-rich phenotype, (TCFA or ThCFA) that caused MACE-R during the follow-up period and a 4-fold sample of lesions with a lipid-rich phenotype that remained quiescent. Lesions with a short length (<9mm), those with suboptimal angiographic images (i.e., poor opacification of lumen silhouette, excessive foreshortening or overlapping), and cases where the DICOM file did not include all the necessary information for 3D-QCA reconstruction were excluded from the analysis.

VH-IVUS data analysis was performed by independent core-laboratories (Cardiovascular Research Foundation, New York, NY in PROSPECT and Cardialysis B.V., Rotterdam, The Netherlands in IBIS 4). Classification of remodeling pattern and lesion phenotype was performed in both core-laboratories using the same protocol (Supplementary file). For each lesion with a TCFA or ThCFA phenotype its remodeling pattern, its length, the length of the proximal shoulder of the lesion, the distance ostium of the studied vessel to minimum lumen area (MLA) of the lesion, its MLA, external elastic membrane (EEM), plaque area and the plaque burden (PB) at the MLA were estimated and recorded.

3D-QCA reconstruction, blood flow simulation and data processing

Anatomical landmarks (i.e., side branches) seen in both IVUS and X-ray angiography were used to identify the proximal and distal end of the *"segment of interest"* (i.e., the segment that was assessed by VH-IVUS) on coronary angiography. Two end-diastolic angiographic projections (>25º apart), where there was no overlapping or foreshortening of the segment of interest and allowed accurate delineation of the lumen silhouette were selected and used to reconstruct its anatomy using well-validated software (QAngio XA 3D RE, Medis, Leiden, the Netherlands) (8). The distance proximal end of the segment of interest to proximal end of each TCFA/ThCFA and distal end of the segment of interest to distal end of each TCFA/ThCFA were used to identify lesion location in 3D-QCA models and then for each lesion 3D-QCA analysis was performed and the lesion length, minimum lumen diameter (MLD) and % DS were estimated.

The 3D-QCA models were processed with computational fluid dynamic techniques and the ESS distribution was estimated (Supplementary file). The location of each TCFA/ThCFA lesion was identified in the 3D-QCA models, the lesion was then divided in consecutive 3mm segments and for each of these segments the ESS values were extracted across the circumference and length of the segment and the mean value was calculated (3,4). For each

lesion the highest and lowest mean ESS values, estimated in the 3mm segments of the lesion, were recorded and defined the "maximum" and "minimum" lesion ESS respectively.

Statistical analysis

Numerical variables are presented as median and interquartile range while categorical variables as absolute values and percentages. The Mann-Whitney U test was used to compare numerical variables between lesions associated with MACE-R or MACE and those that remained quiescent, while categorical variables were compared using the chi-square test. Cox regression analysis was used to identify VH-IVUS, 3D-QCA and 3D-QCA-derived hemodynamic predictors associated with MACE-R or MACE. Receiver-operating characteristics curve analysis was performed for each variable associated with MACE-R ($P<0.05$) and these with the highest area under the curve, that were not collinear ($r<0.5$), were entered into a multivariate model.

Receiver-operating characteristics curve analysis was also used for the computational fluid dynamic-derived variables to identify the best cut-off that predicted MACE-R and this was used to classify lesions in groups. Kaplan-Meier plots were used to display time to event at a lesion and patient level; comparison of the MACE-R rate between groups with different plaque characteristics and hemodynamic profile was performed using the log-rank test. Lesions or patients with no events were censored at the latest contact date. In case of multiple lesions in the same patient, the lesion with the highest maximum ESS value, or the lesion that exhibited the highest pressure gradient was used in the patient level analysis. Analyses were performed in Stata (version 15.1, StataCorp LP, College Station, TX) and R (version 3.4.2, R Foundation for Statistical Computing, Vienna). A P-value <0.05 was considered statistically significant.

Results

Patient demographics

In the PROSPECT study 54 MACE occurred during a median of 3.4 years follow-up. In the IBIS 4 study 15 MACE-R occurred (9 cardiac events and 6 revascularizations) within 5 years follow-up. After excluding cases where IVUS analysis or co-registration with coronary angiography were not possible, cases where there was insufficient information for 3D-QCA reconstruction in the DICOM files, lesions with short length and those with a non-lipid-rich phenotype, 28 MACE-R lesions (n=26 patients) were included in the present analysis [16 from the PROSPECT study and 12 from the IBIS 4 study of which in 6 revascularisation was performed during invasive assessment at 13-month follow-up either because of new onset angina and a 70%≥%DS≥50% (n=1) or significant disease progression (DS>70%, n=5) in follow-up coronary angiography] (Figure 1).

The control group consisted of the non-MACE lipid-rich lesions included in the PROSPECT ESS sub-study investigating the efficacy of the ESS, estimated in IVUS-based models, in predicting events (n=122) (4), and of the non-MACE-R lesions with a lipid-rich phenotype (n=74) identified in the patients that were recruited in the IBIS 4 study at Bern University Hospital. From these lesions, 16 cases were excluded because of sub-optimal angiographic image quality and 61 because of lack of sufficient information in the DICOM file for 3D-QCA analysis; therefore, the final control group consisted of 119 non-MACE-R lipid-rich lesions (53 from the PROSPECT and 66 from the IBIS 4 study; Figure 1).

In total 92 patients (45 recruited in the PROSPECT and 47 in the IBIS 4 study; 119 vessels) were included in the present analysis. As it is shown in Table 1 there were no significant differences in the baseline demographics between the patients who experienced MACE-R and the control group. The baseline demographics of the patients recruited in the PROSPECT and IBS 4 studies are shown in Supplementary Table 1.

Lesions' characteristics and endothelial shear stress distribution

Coronary reconstruction and blood flow simulation was successfully performed in all the studied vessels (n=147). The median length of the reconstructed segment was 44.1 (34.3, 56.2)mm yielding 1882 3mm segments; the median mean ESS was 2.19 (1.46, 3.39)Pa. The IVUS MLA coincided with the 3D-QCA MLA in 40% of the studied lesions; in the remaining lesions IVUS MLA was located in a different 3mm segment than the 3D-QCA MLA. The distribution of the ESS across the studied lesions is shown in the Supplementary Figure 1.

Table 2 shows the morphological, angiographic and hemodynamic characteristics of the studied lesions. MACE-R lesions were longer on VH-IVUS, had a smaller MLA and increased PB comparing to non-MACE-R lesions. Conversely the 3D-QCA lesion length was not different between groups, however the lesions associated with MACE-R had a higher %DS and a smaller MLD. The maximum ESS values and the pressure drop across the MACE-R lesions were higher comparing to non-MACE-R lesions. There were no differences between groups in the incidence of TCFA, the minimum ESS values and the location of MACE-R and non-MACE-R lesions in the coronary tree. Similar findings were noted for the morphological, angiographic and hemodynamic characteristics of the lesions that caused MACE (n=22; Supplementary Table 2).

Predictors of MACE-R and MACE – lesion level analysis

Three VH-IVUS-derived variables (lesion length, MLA and PB), two 3D-QCA-derived variables (MLD and %DS) and two hemodynamic variables (maximum ESS value, pressure drop across the lesion) were predictors of MACE-R lesions (Table 3). By multivariable analysis the PB and the maximum ESS were independent predictors of MACE-R lesions. Maximum ESS was the only independent predictor of MACE-R when the MLA was entered in the multivariate model (HR: 1.08, 95% CI: 1.02, 1.16; P=0.016). Similar results were

reported when analysis was performed only for lesions with a TCFA phenotype (Supplementary Table 3).

The best maximum ESS cut-off for predicting MACE-R lesions was 4.95Pa while the best cut-off for the pressure drop was 2.31mmHg. Lesions were classified in 4 groups according to the presence of ≥2 out of the 3 high-risk plaque characteristics that in the PROSPECT study were associated with MACE (MLA ≤4mm^2, PB ≥70%, TCFA phenotype) and the maximum ESS value (above or below 4.95Pa) (9). As shown in the Figure 2 panel A, lesions with a high-risk plaque morphology exposed to high ESS had worse prognosis than the lesions exposed to high ESS with a low-risk morphology or those exposed to low ESS. The results were not different when a high-risk plaque phenotype was defined as the presence of MLA ≤4mm^2 and PB ≥70% or when the pressure gradient across the lesion (>2.31mmHg) was used to define an unfavourable hemodynamic environment (Figure 2B, 2C, 2D). The additive value of the maximum lesion ESS over the established VH-IVUS-derived high-risk plaque characteristics in predicting MACE-R is shown in Figure 3 and in the Central illustration.

Similar results were reported when analysis was performed for the MACE lesions: VH-IVUS-derived MLA and PB, and 3D-QCA-derived MLD, %DS, maximum ESS and the pressure gradient were predictors of MACE; in multivariate analysis PB and maximum ESS were the only independent predictor of MACE (Table 4). Maximum ESS was the only independent predictor of MACE when the MLA was entered into the multivariate model (HR: 1.09, 95%CI: 1.02, 1.17; P=0.011). The Kaplan-Meier analysis of the MACE rate according to lesion morphological characteristics and maximum ESS or pressure gradient across the lesion is shown in Figure 4.

Predictors of MACE-R – patient level analysis

At a patient level MLA, PB, MLD, %DS and the maximum ESS were predictors of MACE-R (Supplementary Table 4). Patients that had lipid-rich plaques with ≥2 high-risk plaque characteristics that were exposed to high ESS (>4.95Pa) had worse prognosis than those with high-risk plaques exposed to low ESS (Figure 5). The pressure gradient across the lesion also appeared to provide additional prognostic information to plaque morphology; patients with lesions with ≥2 high-risk plaque characteristics that exhibited a pressure gradient >2.31mmHg had the worst prognosis compared to the other groups. Similar results were reported when high-risk lesions were defined as those with MLA ≤4mm^2 and PB ≥70%.

Discussion

The present study for the first time evaluated the prognostic utility of the 3D-QCA-derived hemodynamic indices and plaque characteristics in stratifying non-flow limiting lesions that are likely to progress and cause MACE-R or MACE. We found that 1) ESS distribution estimated in 3D-QCA models provided additional prognostic information and was an independent predictor of MACE-R or MACE, 2) the pressure gradient across non-flow limiting lipid-rich lesions was a predictor of MACE-R/MACE, 3) the combination of plaque characteristics and 3D-QCA-derived hemodynamic indices (i.e., ESS or the pressure gradient across the lesion) enabled more accurate detection of MACE-R and MACE lesions than VH-IVUS-derived variables, and that 4) plaque morphology and the hemodynamic variables estimated in 3D-QCA models allowed more accurate identification of the patients who were at risk to suffer a cardiovascular event than standalone VH-IVUS imaging.

Computational fluid dynamic-based animal and human studies have provided robust evidence about the role of the local hemodynamic forces on atherosclerotic disease progression and highlighted their prognostic implications (10). Low ESS appears to promote, through mechanotransduction pathways, plaque evolution and the development of high-risk plaques

and in clinical studies it has been reported to be a predictor of lesions that progressed and caused events (3,11). Conversely, the role of high ESS on the formation of high-risk plaques is less well established; however there is considerable evidence to suggest that high ESS contributes to the destabilization of vulnerable lesions (12,13). Despite the undoubted prognostic implications of ESS, blood flow simulation analyses have limited applications in the clinical arena. This should be at least partially attributed to the increased time required for coronary reconstruction and blood flow modelling.

In the present study we examined the prognostic value of 3D-QCA-derived hemodynamic variables in detecting non-flow limiting lipid-rich plaques that are likely to progress and cause MACE-R. In contrast to what has been reported in previous studies we found that the maximum and not the minimum ESS predicted MACE-R and MACE (3,4). This discrepancy may be attributed to the different modality used to extract vessel geometry; 3D-QCA modelling has limited efficacy in assessing details in lumen morphology, which can affect ESS estimations especially in complex long lesions that are likely to exhibit ESS heterogeneity (14). Indeed, in the present study in which the median lesion length was 22.7mm, the IVUS and 3D-QCA MLA co-located in only 40% of lesions, a finding which highlights the limited accuracy of 3D-QCA to accurately extract lumen architecture (Supplementary Figure 2). Taking into account the limitations of 3D-QCA and the fact that it generates smooth luminal surfaces, in the present study we used the mean rather the more commonly used minimum predominant ESS value to define the physiologic profile of the 3mm segments (3,4).

Despite the limitations of 3D-QCA-modelling, the estimated hemodynamic indices, and in particular the ESS distribution provided useful prognostic information and improved the efficacy of established VH-IVUS-derived plaque characteristics in predicting events (Figure 3 and Central illustration). The maximum ESS was a predictor of lesion-related MACE-

R/MACE in multivariable analysis, and the Kaplan-Meier plots demonstrated the synergetic effect of plaque morphology and ESS in predicting future MACE or angiographically indicated revascularizations. Two recent studies, the EMERALD (Exploring the MEchanism of plaque Rupture in Acute coronary syndrome using coronary CT Angiography and computationaL fluid Dynamics) and a post hoc analysis from the FAME II reported similar findings to our analysis, demonstrating that the maximum ESS estimated in lesions reconstructed by CTCA or 3D-QCA were predictors of future myocardial infarctions (6,15). These studies however, included predominately flow limiting lesions (49% and 100% of the lesions included in the EMERALD and FAME II studies respectively had fractional flow reserve $\leq$0.80) that should have been considered for revascularization. Conversely, our analysis focused on non-flow limiting stenoses, with a median pressure gradient across these lesions of only 1.95 (1.14, 3.33)mmHg, for which there is lack of evidence to support their invasive passivation. In addition, the EMERALD study included predominately patients without a previous history of coronary artery disease who are less likely to have complex lesions, while in the FAME II study there was no information about plaque composition and therefore this analysis was unable to examine the additive predictive value of hemodynamic indices over anatomical and morphological plaque characteristics derived by intravascular imaging. Finally, coronary reconstruction and blood flow simulation in both studies was computationally demanding as the EMERALD used computed tomographic coronary angiography derived models while the FAME II study incorporated the side branches in the 3D-QCA models which increases considerably the computation time. Conversely our analysis included only the main branch and assumed steady coronary flow; this approach makes feasible the real-time estimation of the ESS while the patient is on the catheterisation laboratory.

The unfavourable implications of high ESS on plaque pathobiology is supported by several experimental studies which have shed light into the mechanotransduction pathways that regulate plaque evolution. High ESS promotes nitric oxide synthesis and proteolytic degradation of the fibrous cap by inhibiting extracellular matrix synthesis, and increases smooth muscle cell apoptosis and proteolytic matrix degradation (10). The above processes eventually result in fibrous cap fragility and rupture which can cause vessel thrombosis or plaque healing with accelerated disease progression (16). These events can have clinical manifestations if they occur in segments with increased PB and small MLA as in this setting they are likely to cause flow obstruction and ischemia (17). Indeed, in our study apart from the ESS increased PB and small MLA were also predictors of MACE-R while PB was an independent predictor of MACE-R in multivariate Cox regression analysis as well. Interestingly, apart from the ESS, the pressure gradient across the lesion estimated in our 3D-QCA models also provided useful prognostic information and was a predictor of MACE-R and MACE. Kaplan-Meier analysis showed that lesions with a high pressure gradient (and especially these with high-risk plaque characteristic) had a poor prognosis with event rates as high as 51.8% at 5-year follow-up. Several studies have demonstrated that a low fractional flow reserve is a predictor of worse outcomes even in angiographically non-flow limiting stenoses (15). In these studies, the prognostic value of fractional flow reserve has been attributed to the fact that it reflects atherosclerotic burden. In our analysis however, and in the EMERALD study, the pressure gradient seemed to provide additional prognostic information beyond plaque characteristics. An increased pressure gradient across a lesion has been associated with increased axial tensile stress, flow disturbances and ESS heterogeneity; this unfavourable hemodynamic environment can accelerate atherosclerotic evolution leading to plaque destabilization and future events (18,19).

The findings of the present analysis provide evidence of the value of 3D-QCA-derived hemodynamic indices in identifying vulnerable plaques (Supplementary Figure 3). Software have been developed that enable real-time computation of the fractional flow reserve from 3D-QCA, which may be used in future studies to enhance the efficacy of intravascular imaging in detecting plaques prone to progress and cause events (20).

Moreover, the present analysis also underscores the potential value of plaque morphology and physiology (i.e., ESS distribution or pressure drop across a lesion) in stratifying cardiovascular risk. The models that are currently available to identify high-risk patients rely either on patient demographics or on the combination of clinical and imaging biomarkers and have modest predictive accuracy (21). The patient-level analysis of our study showed that the subjects with high-risk plaques and an unfavourable local hemodynamic environment had a high event rate during follow-up. Further research is needed to examine the potential value of non-invasive or invasive assessment of plaque pathology (i.e., plaque burden and composition) and physiology in identifying patients at risk who would benefit from emerging therapies targeting atherosclerosis.

Limitations

A significant limitation of the present analysis is the fact that only 48% of the lipid-rich lesions that caused MACE-R were suitable for inclusion; this may have introduced selection bias and resulted in a small sample size and events that did not allow us to accurately quantify the additive value of hemodynamic variables over VH-IVUS-derived plaque characteristics in predicting MACE-R. Therefore, the reported results should be interpreted with caution and require further confirmation in future large scale studies.

In addition, in some of the angiograms from the PROSPECT study the pixel size was not available and thus vessel reconstruction relied on a manual calibration which can affect the

accuracy of 3D-QCA modelling. Additionally, we performed steady flow simulation, assuming that the blood was a Newtonian fluid and we did not include side branches in the 3D-QCA models. Steady flow simulation can accurately predict time averaged ESS in pulsatile simulations (22). Conversely a Newtonian assumption may not accurately approximate blood behaviour, especially in diseased segments where more regions of slow flow are expected (23). In addition, the incorporation of the side branches in the 3D models is expected to enable more accurate assessment of the ESS distribution; however a recent study has shown that the incorporation of the side branches on the 3D vessel geometry only marginally improved the accuracy of the ESS in predicting plaque evolution (24). Complex simulation especially in complex geometries is time consuming and cannot be performed in the catheterisation laboratory. With the proposed approach ESS and especially the pressure drop across a lesion can be computed fast in single vessel geometries; currently QCA reconstruction and blood flow simulation takes ~15min, however developments in software design and advances in computer technology are expected to reduce this time to few minutes enabling the real-time computation of 3D-QCA-derived ESS.

Furthermore, VH-IVUS imaging was performed using two different imaging systems (Invision Gold in PROSPECT and s5 in IBIS 4); VH analysis from these two systems may provide different estimations for plaque composition and phenotype. In addition, follow-up coronary angiography and revascularisation because of disease progression on angiogram was performed only in the IBIS 4 study, while the follow-up period (median 3.4 years in the PROSPECT and 5 years in the IBIS 4) was different in the two studies. However, it is reassuring that our findings were similar when analysis was restricted to MACE or to the first 3.4 years of follow-up (Supplementary Figure 4).

Finally, the number of the events reported in this analysis was relatively small and most of the events were unstable or progressive angina and not hard clinical endpoints (death,

myocardial infarction). However, it has to be acknowledged that in all the prospective multi-vessel intravascular imaging studies of coronary atherosclerosis the incidence of hard endpoints is low (1-3). In addition, the clinical endpoints of this study are similar to the endpoints of the recently completed Lipid Rich Plaque study and of ongoing studies of coronary atherosclerosis (PROSPECT II, NCT02171065; PREVENT, NCT02316886; COMBINE OCT-FFR, NCT02989740) that are expected to provide additional data and the substrate to prove the concept introduced in this report.

Conclusions

In the present analysis of the PROSPECT and IBIS 4 studies, hemodynamic indices estimated from 3D-QCA models provided additional prognostic information to VH-IVUS-derived variables and enabled more accurate detection of non-flow limiting lesions that are likely to progress and cause events. Prospective studies are needed to confirm these findings and examine the efficacy of intravascular imaging and 3D-QCA-derived variables in detecting high-risk lesions and patients who may benefit from pre-emptive focal or systemic treatment of atherosclerosis.

Perspectives

Competency in medical knowledge: In this post-hoc analysis of the PROSPECT and IBIS 4 imaging studies the ESS estimated in 3D-QCA-derived models improved the predictive efficacy of VH-IVUS in identifying lesions prone to exhibit disease progression and cause MACE-R at 5 year follow-up.

Translational outlook: Future developments in software design are expected to enable fast computation of the ESS distribution in 3D-QCA models and facilitate the conduction of large

scale studies that will assess the potential value of 3D-QCA-derived ESS in predicting lesions that are likely to progress and cause cardiovascular events.

References

1. Waksman R. Assessment of coronary near-infrared spectroscopy imaging to detect vulnerable plaques and vulnerable patients. The Lipid-Rich Plaque study. Transcatheter Cardiovascular Theurapeutics 2018;21-25 September.
2. Stone GW, Maehara A, Lansky AJ et al. A prospective natural-history study of coronary atherosclerosis. N Engl J Med 2011;364:226-35.
3. Stone PH, Saito S, Takahashi S et al. Prediction of progression of coronary artery disease and clinical outcomes using vascular profiling of endothelial shear stress and arterial plaque characteristics: the PREDICTION Study. Circulation 2012;126:172-81.
4. Stone PH, Maehara A, Coskun AU et al. Role of Low Endothelial Shear Stress and Plaque Characteristics in the Prediction of Nonculprit Major Adverse Cardiac Events: The PROSPECT Study. JACC Cardiovasc Imaging 2018;11:462-471.
5. Bourantas CV, Ramasamy A, Karagiannis A et al. Angiographic derived endothelial shear stress: a new predictor of atherosclerotic disease progression. Eur Heart J Cardiovasc Imaging 2018.
6. Kumar A, Thompson EW, Lefieux A et al. High Coronary Shear Stress in Patients With Coronary Artery Disease Predicts Myocardial Infarction. J Am Coll Cardiol 2018;72:1926-1935.
7. Raber L, Taniwaki M, Zaugg S et al. Effect of high-intensity statin therapy on atherosclerosis in non-infarct-related coronary arteries (IBIS-4): a serial intravascular ultrasonography study. Eur Heart J 2015;36:490-500.
8. Tu S, Huang Z, Koning G, Cui K, Reiber JH. A novel three-dimensional quantitative coronary angiography system: In-vivo comparison with intravascular ultrasound for assessing arterial segment length. Catheter Cardiovasc Interv 2010;76:291-8.
9. Stone GW, Maehara A, Lansky AJ et al. A prospective natural-history study of coronary atherosclerosis. N Engl J Med 2011;364:226-35.
10. Thondapu V, Bourantas CV, Foin N, Jang IK, Serruys PW, Barlis P. Biomechanical stress in coronary atherosclerosis: emerging insights from computational modelling. Eur Heart J 2017;38:81-92.
11. Chatzizisis YS, Baker AB, Sukhova GK et al. Augmented expression and activity of extracellular matrix-degrading enzymes in regions of low endothelial shear stress colocalize with coronary atheromata with thin fibrous caps in pigs. Circulation 2011;123:621-30.
12. Torii R, Stettler R, Raber L et al. Implications of the local hemodynamic forces on the formation and destabilization of neoatherosclerotic lesions. Int J Cardiol 2018;272:7-12.
13. Fukumoto Y, Hiro T, Fujii T et al. Localized elevation of shear stress is related to coronary plaque rupture: a 3-dimensional intravascular ultrasound study with in-vivo color mapping of shear stress distribution. J Am Coll Cardiol 2008;51:645-50.
14. Antoniadis AP, Papafaklis MI, Takahashi S et al. Arterial Remodeling and Endothelial Shear Stress Exhibit Significant Longitudinal Heterogeneity Along the Length of Coronary Plaques. JACC Cardiovasc Imaging 2016;9:1007-9.
15. Lee JM, Koo BK, Shin ES et al. Clinical implications of three-vessel fractional flow reserve measurement in patients with coronary artery disease. Eur Heart J 2018;39:945-951.
16. Davies MJ, Thomas AC. Plaque fissuring--the cause of acute myocardial infarction, sudden ischaemic death, and crescendo angina. Br Heart J 1985;53:363-73.
17. Tian J, Ren X, Vergallo R et al. Distinct morphological features of ruptured culprit plaque for acute coronary events compared to those with silent rupture and thin-cap fibroatheroma: a combined optical coherence tomography and intravascular ultrasound study. J Am Coll Cardiol 2014;63:2209-16.
18. Park JB, Choi G, Chun EJ et al. Computational fluid dynamic measures of wall shear stress are related to coronary lesion characteristics. Heart 2016;102:1655-61.

19. Slager CJ, Wentzel JJ, Gijsen FJ et al. The role of shear stress in the destabilization of vulnerable plaques and related therapeutic implications. Nat Clin Pract Cardiovasc Med 2005;2:456-64.
20. Bourantas CV, Garcia-Garcia HM, Diletti R, Muramatsu T, Serruys PW. Early detection and invasive passivation of future culprit lesions: a future potential or an unrealistic pursuit of chimeras? Am Heart J 2013;165:869-881 e4.
21. Bourantas CV, Garcia-Garcia HM, Torii R et al. Vulnerable plaque detection: an unrealistic quest or a feasible objective with a clinical value? Heart 2016;102:581-9.
22. Feldman CL, Ilegbusi OJ, Hu Z, Nesto R, Waxman S, Stone PH. Determination of in vivo velocity and endothelial shear stress patterns with phasic flow in human coronary arteries: a methodology to predict progression of coronary atherosclerosis. Am Heart J 2002;143:931-9.
23. Liu B, Tang D. Influence of non-Newtonian properties of blood on the wall shear stress in human atherosclerotic right coronary arteries. Mol Cell Biomech 2011;8:73-90.
24. Sakellarios A, Bourantas CV, Papadopoulou SL et al. The effect of coronary bifurcation and haemodynamics in prediction of atherosclerotic plaque development: a serial computed tomographic coronary angiographic study. EuroIntervention 2017;13:e1084-e1091.

Figure legends

Figure 1. Study design. Flowchart of the lesions included in the present analysis.

Figure 2. Kaplan-Meier curves showing MACE-R rate according to plaque and 3D-QCA-derived haemodynamic indices. Lesions were classified in groups according to the presence of absence of (A) ≥2 high-risk plaque features and increased maximum ESS values (>4.95Pa), (B) ≥2 high-risk plaque features and high pressure gradient (>2.31mmHg) across the lesion, (C) PB ≥70%, MLA ≤4mm^2 and increased maximum ESS and (D) PB ≥70%, MLA ≤4mm^2 and high pressure gradient.

Figure 3. MACE-R rate of lesions with and without VH-IVUS-derived high-risk plaque characteristics that were or were not exposed to high maximum ESS values. ESS (+) indicates lesions exposed to high maximum ESS (>4.95Pa); TCFA (+) indicates the presence of a TCFA phenotype; MLA (+) a MLA ≤4.0mm^2 and PB (+) a PB ≥70%.

Central illustration. MACE-R rate of lesions with and without VH-IVUS-defined high-risk plaque characteristics exposed to high or low maximum ESS. TCFA (+) indicates the lesions with a TCFA phenotype, MLA (+) the lesions with MLA ≤4.0mm^2, PB (+) the lesions with PB ≥70% and ESS (+) the lesions exposed to high maximum ESS (>4.95Pa).

Figure 4. Kaplan-Meier curves showing MACE rate according to plaque and 3D-QCA-derived haemodynamic indices. Lesions were classified in groups according to the presence of absence of (A) ≥2 high-risk plaque features and increased maximum ESS values (>4.95Pa), (B) ≥2 high-risk plaque features and high pressure gradient (>2.31mmHg) across the lesion, (C) PB ≥70% and MLA ≤4mm^2 and increased maximum ESS values and (D) PB ≥70% and MLA ≤4mm^2 and high pressure gradient.

Figure 5. Kaplan-Meier curves showing patient level MACE-R rate according to plaque and 3D-QCA-derived haemodynamic indices. (A) Patients were classified in groups according to the presence of absence of (A) high-risk plaques (i.e., plaques with ≥2 high-risk features) and increased maximum ESS values (>4.95Pa), (B) high-risk plaques and high pressure gradient (>2.31mmHg) across the lesion, (C) PB ≥70% and MLA ≤4mm^2 and increased maximum ESS values and (D) lesions with PB ≥70%, MLA ≤4mm^2 and high pressure gradient.

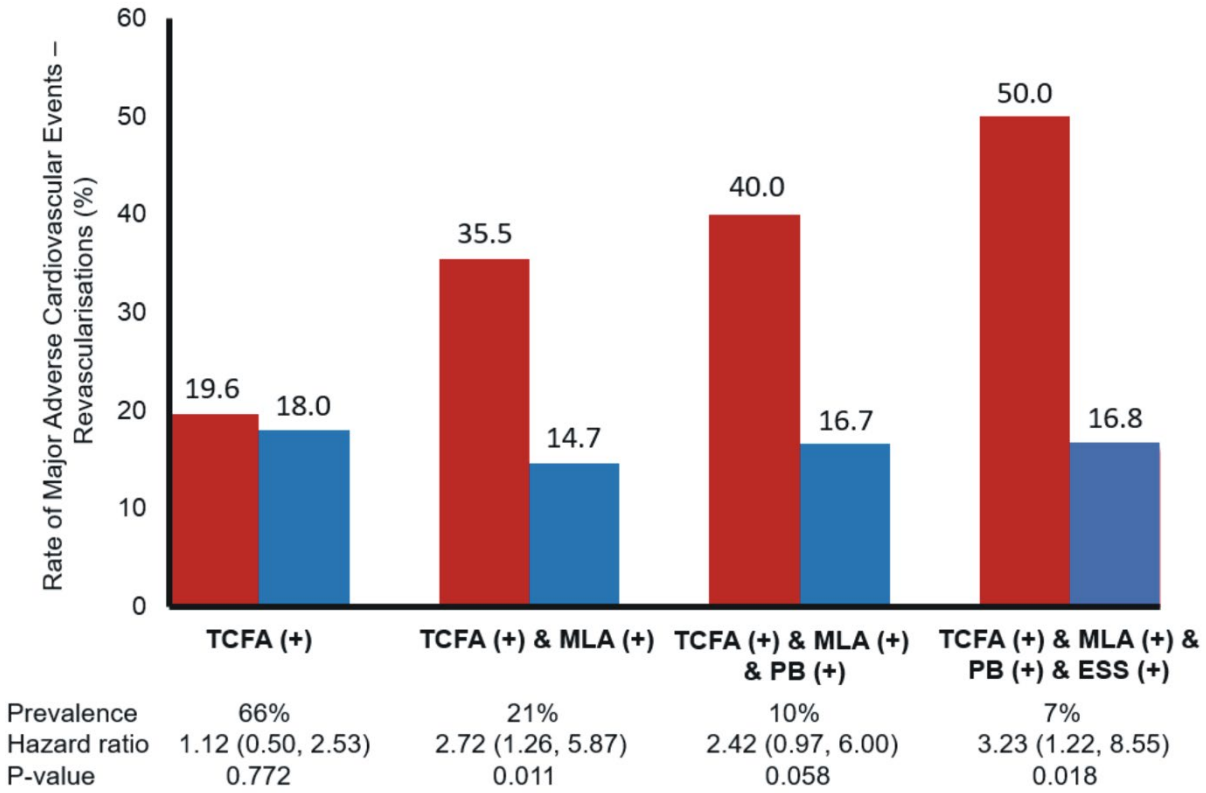

Prevalence	66%	21%	10%	7%
Hazard ratio	1.12 (0.50, 2.53)	2.72 (1.26, 5.87)	2.42 (0.97, 6.00)	3.23 (1.22, 8.55)
P-value	0.772	0.011	0.058	0.018

Central illustration

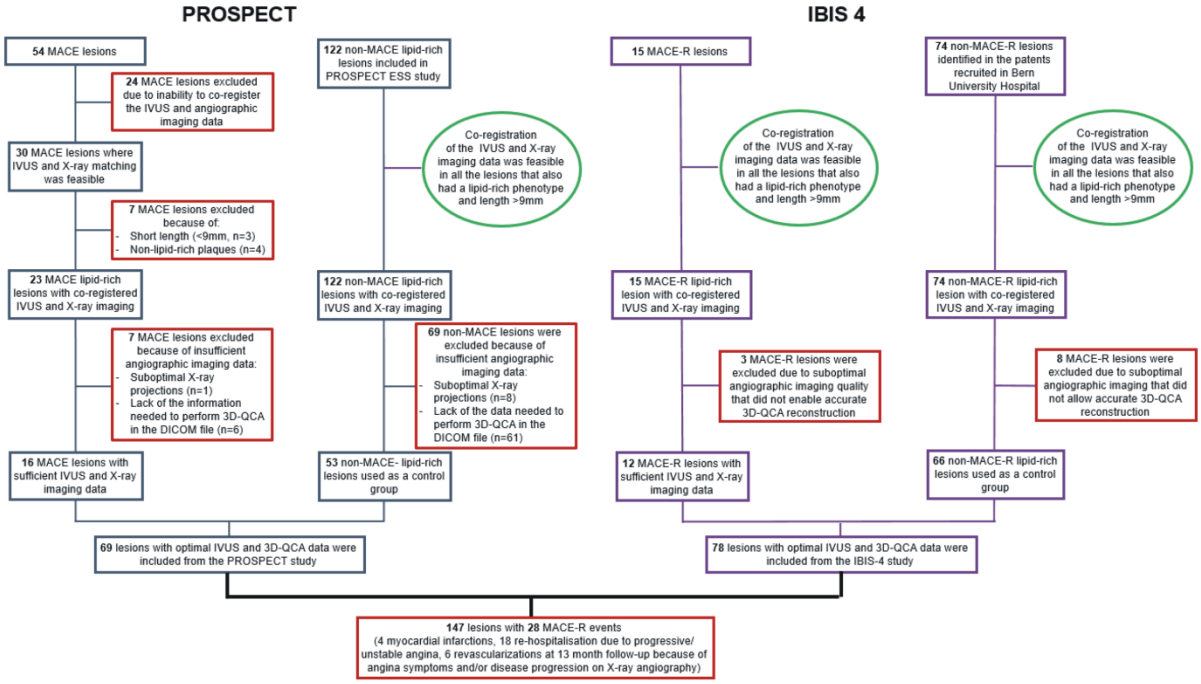

Fig 1.

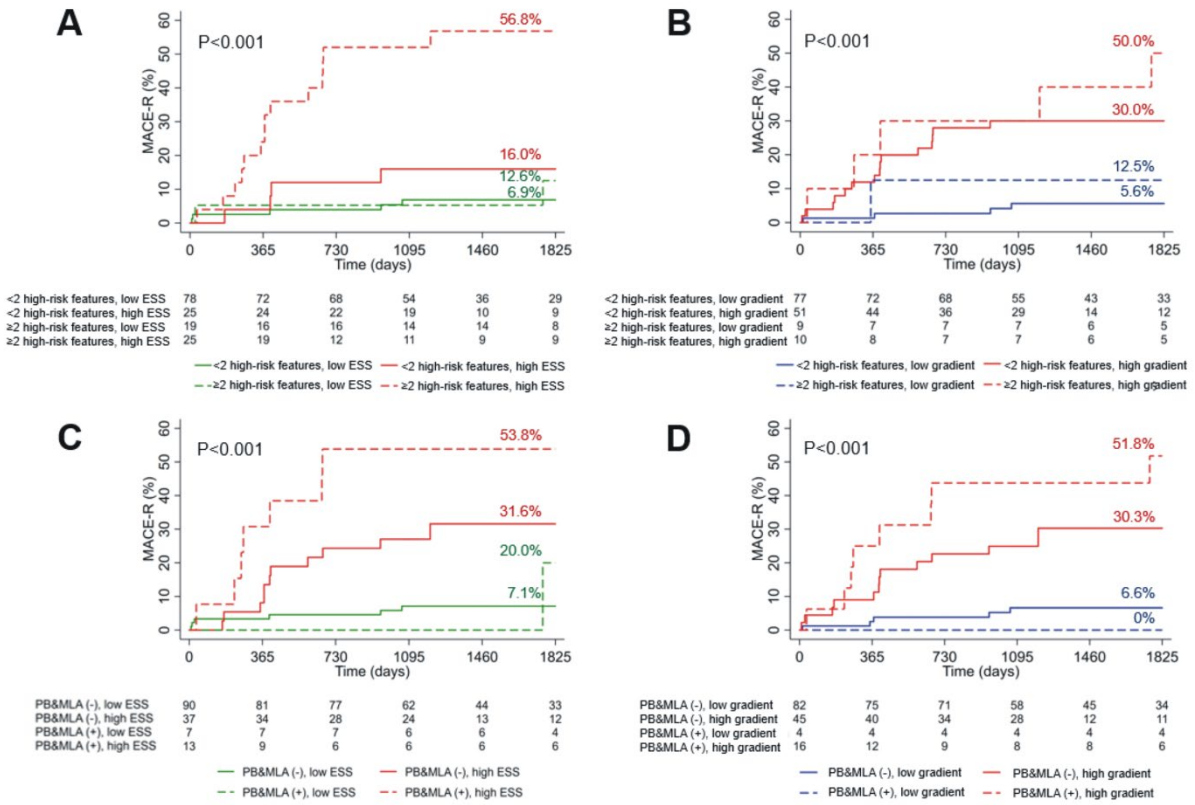
A
P<0.001
56.8%
16.0%
12.6%
6.9%
MACE-R (%)
Time (days)
<2 high-risk features, low ESS 78 72 68 54 36 29
<2 high-risk features, high ESS 25 24 22 19 10 9
≥2 high-risk features, low ESS 19 16 16 14 14 8
≥2 high-risk features, high ESS 25 19 12 11 9 9
<2 high-risk features, low ESS
<2 high-risk features, high ESS
≥2 high-risk features, low ESS
≥2 high-risk features, high ESS
B
P<0.001
50.0%
30.0%
12.5%
5.6%
MACE-R (%)
Time (days)
<2 high-risk features, low gradient 77 72 68 55 43 33
<2 high-risk features, high gradient 51 44 36 29 14 12
≥2 high-risk features, low gradient 9 7 7 7 6 5
≥2 high-risk features, high gradient 10 8 7 7 6 5
<2 high-risk features, low gradient
<2 high-risk features, high gradient
≥2 high-risk features, low gradient
≥2 high-risk features, high gradient
C
P<0.001
53.8%
31.6%
20.0%
7.1%
MACE-R (%)
Time (days)
PB&MLA (-), low ESS 90 81 77 62 44 33
PB&MLA (-), high ESS 37 34 28 24 13 12
PB&MLA (+), low ESS 7 7 7 6 6 4
PB&MLA (+), high ESS 13 9 6 6 6 6
PB&MLA (-), low ESS
PB&MLA (-), high ESS
PB&MLA (+), low ESS
PB&MLA (+), high ESS
D
P<0.001
51.8%
30.3%
6.6%
0%
MACE-R (%)
Time (days)
PB&MLA (-), low gradient 82 75 71 58 45 34
PB&MLA (-), high gradient 45 40 34 28 12 11
PB&MLA (+), low gradient 4 4 4 4 4 4
PB&MLA (+), high gradient 16 12 9 8 8 6
PB&MLA (-), low gradient
PB&MLA (-), high gradient
PB&MLA (+), low gradient
PB&MLA (+), high gradient

Fig 2

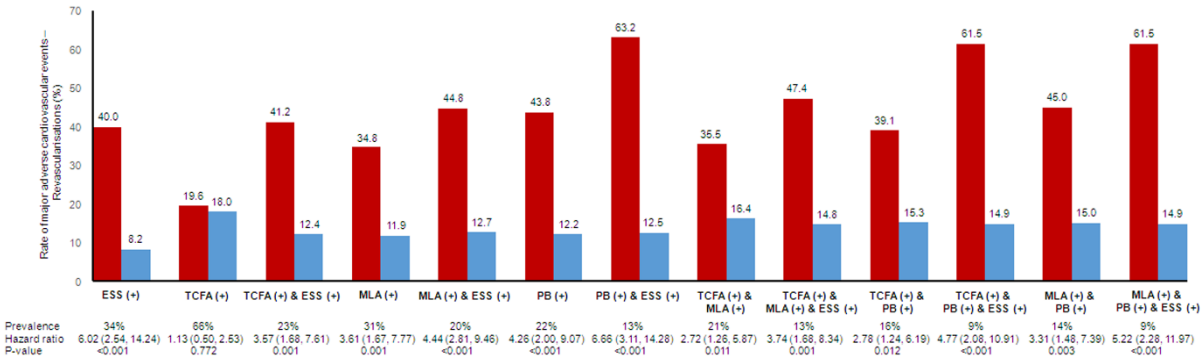
Rate of major adverse cardiovascular events – Revascularisations (%)
40.0
8.2
19.6
18.0
41.2
12.4
34.8
11.9
44.8
12.7
43.8
12.2
63.2
12.5
35.5
16.4
47.4
14.8
39.1
15.3
61.5
14.9
45.0
15.0
61.5
14.9
ESS (+)
TCFA (+)
TCFA (+) & ESS (+)
MLA (+)
MLA (+) & ESS (+)
PB (+)
PB (+) & ESS (+)
TCFA (+) & MLA (+)
TCFA (+) & MLA (+) & ESS (+)
TCFA (+) & PB (+)
TCFA (+) & PB (+) & ESS (+)
MLA (+) & PB (+)
MLA (+) & PB (+) & ESS (+)
Prevalence 34% 66% 23% 31% 20% 22% 13% 21% 13% 16% 9% 14% 9%
Hazard ratio 6.02 (2.54, 14.24) 1.13 (0.50, 2.53) 3.57 (1.68, 7.61) 3.61 (1.67, 7.77) 4.44 (2.81, 9.46) 4.26 (2.00, 9.07) 6.66 (3.11, 14.28) 2.72 (1.26, 5.87) 3.74 (1.68, 8.34) 2.78 (1.24, 6.19) 4.77 (2.08, 10.91) 3.31 (1.48, 7.39) 5.22 (2.28, 11.97)
P-value <0.001 0.772 0.001 0.001 <0.001 <0.001 <0.001 0.011 0.001 0.012 <0.001 0.003 <0.001

Fig 3

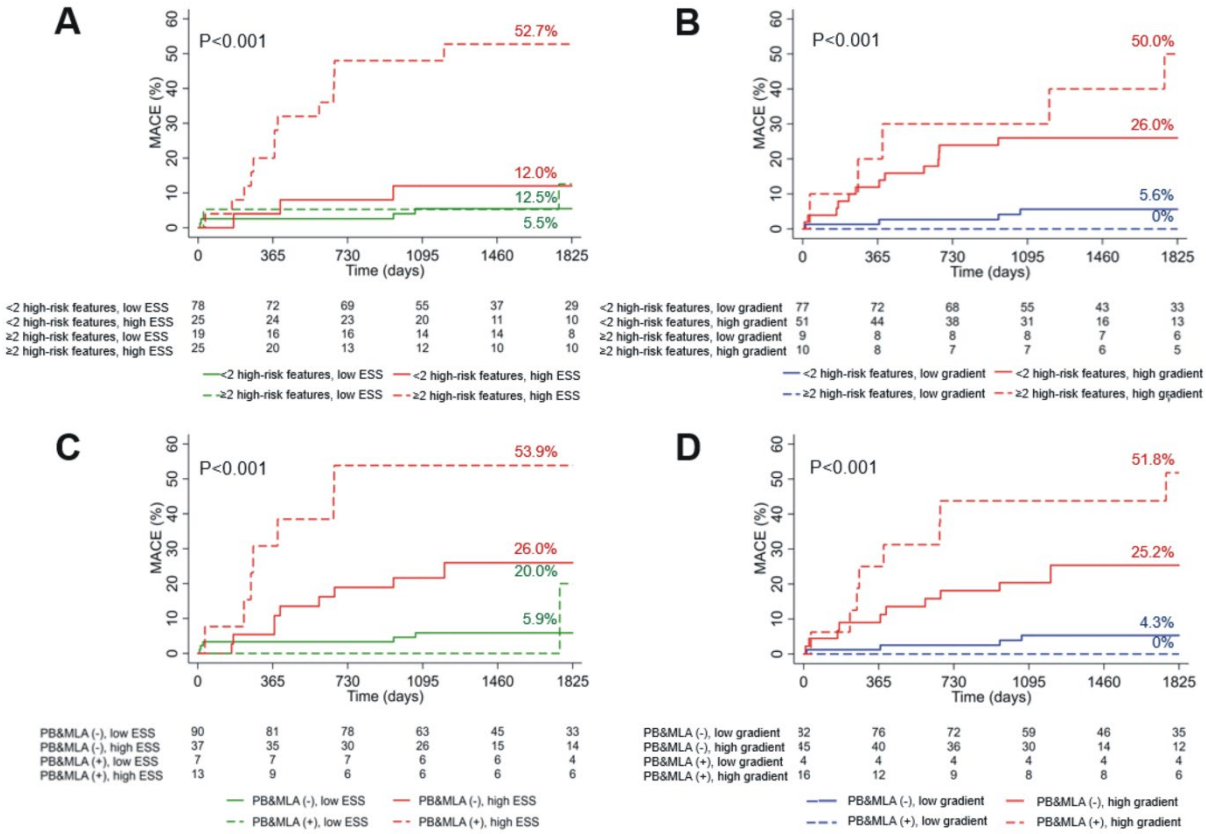
A
P<0.001
52.7%
12.0%
12.5%
5.5%
MACE (%)
Time (days)
<2 high-risk features, low ESS 78 72 69 55 37 29
<2 high-risk features, high ESS 25 24 23 20 11 10
≥2 high-risk features, low ESS 19 16 16 14 14 8
≥2 high-risk features, high ESS 25 20 13 12 10 10
<2 high-risk features, low ESS
<2 high-risk features, high ESS
≥2 high-risk features, low ESS
≥2 high-risk features, high ESS
B
P<0.001
50.0%
26.0%
5.6%
0%
MACE (%)
Time (days)
<2 high-risk features, low gradient 77 72 68 55 43 33
<2 high-risk features, high gradient 51 44 38 31 16 13
≥2 high-risk features, low gradient 9 8 8 8 7 6
≥2 high-risk features, high gradient 10 8 7 7 6 5
<2 high-risk features, low gradient
<2 high-risk features, high gradient
≥2 high-risk features, low gradient
≥2 high-risk features, high gradient
C
P<0.001
53.9%
26.0%
20.0%
5.9%
MACE (%)
Time (days)
PB&MLA (-), low ESS 90 81 78 63 45 33
PB&MLA (-), high ESS 37 35 30 26 15 14
PB&MLA (+), low ESS 7 7 7 6 6 4
PB&MLA (+), high ESS 13 9 6 6 6 6
PB&MLA (-), low ESS
PB&MLA (-), high ESS
PB&MLA (+), low ESS
PB&MLA (+), high ESS
D
P<0.001
51.8%
25.2%
4.3%
0%
MACE (%)
Time (days)
PB&MLA (-), low gradient 32 76 72 59 46 35
PB&MLA (-), high gradient 45 40 36 30 14 12
PB&MLA (+), low gradient 4 4 4 4 4 4
PB&MLA (+), high gradient 16 12 9 8 8 6
PB&MLA (-), low gradient
PB&MLA (-), high gradient
PB&MLA (+), low gradient
PB&MLA (+), high gradient

Fig 4

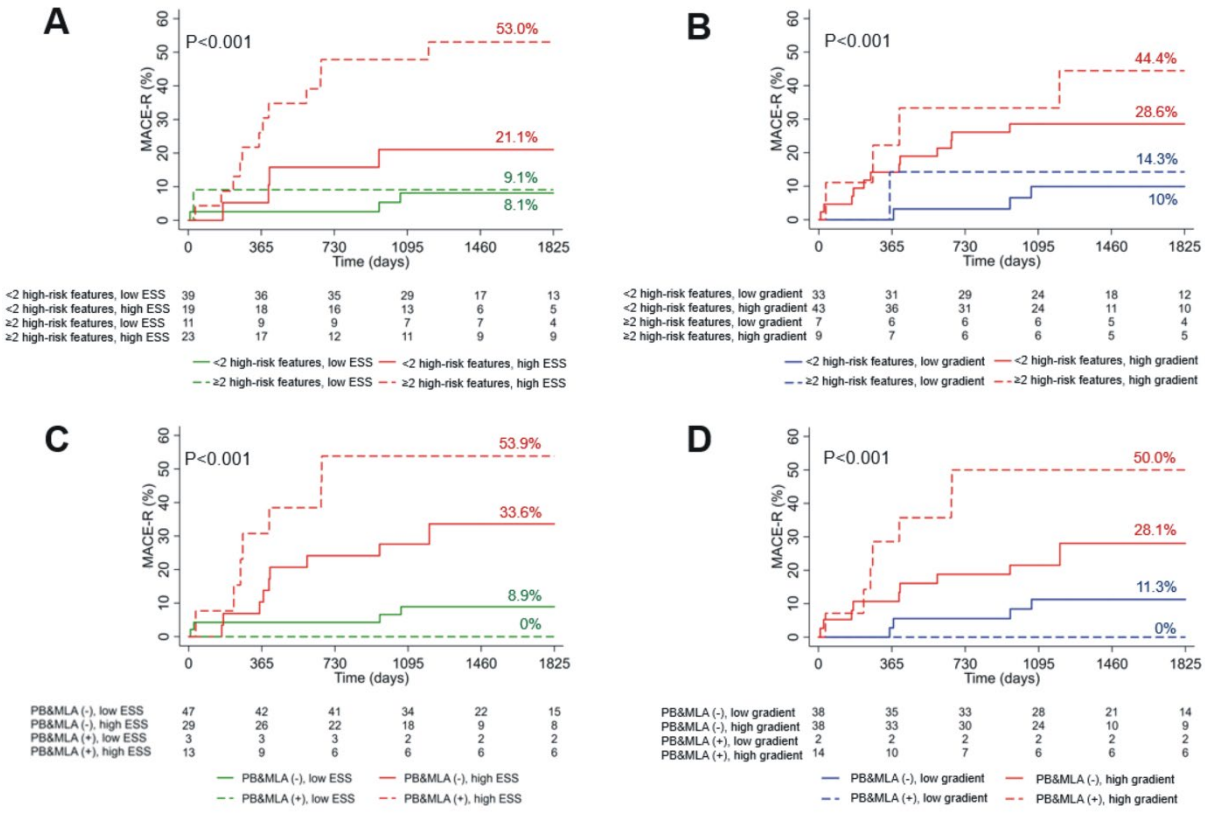
A
P<0.001
53.0%
21.1%
9.1%
8.1%
MACE-R (%)
Time (days)
<2 high-risk features, low ESS 39 36 35 29 17 13
<2 high-risk features, high ESS 19 18 16 13 6 5
≥2 high-risk features, low ESS 11 9 9 7 7 4
≥2 high-risk features, high ESS 23 17 12 11 9 9
<2 high-risk features, low ESS
<2 high-risk features, high ESS
≥2 high-risk features, low ESS
≥2 high-risk features, high ESS
B
P<0.001
44.4%
28.6%
14.3%
10%
MACE-R (%)
Time (days)
<2 high-risk features, low gradient 33 31 29 24 18 12
<2 high-risk features, high gradient 43 36 31 24 11 10
≥2 high-risk features, low gradient 7 6 6 6 5 4
≥2 high-risk features, high gradient 9 7 6 6 5 5
<2 high-risk features, low gradient
<2 high-risk features, high gradient
≥2 high-risk features, low gradient
≥2 high-risk features, high gradient
C
P<0.001
53.9%
33.6%
8.9%
0%
MACE-R (%)
Time (days)
PB&MLA (-), low ESS 47 42 41 34 22 15
PB&MLA (-), high ESS 29 26 22 18 9 8
PB&MLA (+), low ESS 3 3 3 2 2 2
PB&MLA (+), high ESS 13 9 6 6 6 6
PB&MLA (-), low ESS
PB&MLA (-), high ESS
PB&MLA (+), low ESS
PB&MLA (+), high ESS
D
P<0.001
50.0%
28.1%
11.3%
0%
MACE-R (%)
Time (days)
PB&MLA (-), low gradient 38 35 33 28 21 14
PB&MLA (-), high gradient 38 33 30 24 10 9
PB&MLA (+), low gradient 2 2 2 2 2 2
PB&MLA (+), high gradient 14 10 7 6 6 6
PB&MLA (-), low gradient
PB&MLA (-), high gradient
PB&MLA (+), low gradient
PB&MLA (+), high gradient

Fig 5

Table 1. Baseline demographics of the patients who experienced MACE-R and of the control group.

	Studied patients (N=92)	Patients that had MACE-R (N=26)	Control group (N=66)	P
Age (years)	58.2 (51.5, 64.8)	60.5 (53.5, 67.0)	57.4 (50.9, 64.3)	0.422
Gender (male)	81 (88%)	24 (92%)	57 (86%)	0.429
BMI	27.1 (24.4, 30.1)	27.5 (24.6, 31.0)	27.0 (24.2, 29.9)	0.643
Current smoker	47 (47%)	14 (54%)	27 (41%)	0.261
Co-morbidities				
Diabetes mellitus	15 (17%)	7 (27%)	9 (14%)	0.130
Hypertension	42 (46%)	11 (44%)	31 (47%)	0.800
Hypercholesterolemia	36 (40%)	10 (44%)	26 (39%)	0.731
Renal failure*	3 (3%)	1 (4%)	2 (3%)	0.764
Previous PCI	6 (7%)	3 (11%)	3 (4%)	0.221
Family history of CAD	30 (33%)	9 (39%)	21 (33%)	0.585
Clinical presentation				**0.961**
STEMI	58 (63%)	16 (61%)	42 (64%)	
NSTEMI	30 (33%)	9 (35%)	21 (32%)	
Unstable angina	4 (4%)	1 (4%)	3 (4%)	
Medications at discharge				
Aspirin	91 (99%)	26 (100%)	65 (98%)	0.528
Thienopyridines	92 (100%)	100 (100%)	45 (100%)	-
Beta-blocker	87 (95%)	23 (89%)	64 (97%)	0.105
RAAS inhibitor	76 (83%)	20 (77%)	56 (85%)	0.367
Statin	88 (96%)	25 (96%)	63 (95%)	0.882

Table footnote: BMI, body mass index; CAD, coronary artery disease; NSTEMI, non ST-elevation myocardial infarction; PCI, percutaneous coronary intervention; RAAS, renin angiotensin aldosterone system; STEMI, ST-elevation myocardial infarction.

*Renal failure was defined as estimated glomerular filtration rate <60mL/min/1.73m^2

Table 2. Morphological and hemodynamic characteristics of the MACE-R lesions and of these that remained quiescent during follow-up.

	Studied lesions (N=147)	MACE-R lesions (N=28)	Non-MACE-R lesions (N=119)	P
VH-IVUS plaque characteristics				
VH-IVUS lesion length (mm)	22.7 (12.9, 35.2)	32.5 (18.0, 41.6)	19.6 (12.7, 31.3)	0.030
Distance vessel ostium to MLA (mm)	24.2 (10.2, 35.9)	29.8 (15.1, 44.6)	23.8 (9.2, 34.3)	0.088
Length of the proximal shoulder (mm)	11.3 (6.6, 23.1)	12.5 (6.5, 18.2)	10.6 (6.6, 23.3)	0.892
MLA (mm^2)	4.81 (3.68, 6.30)	3.65 (3.26, 4.36)	5.03 (3.98, 6.66)	<0.001
EEM area (mm^2)	13.39 (10.53, 16.11)	11.60 (10.64, 14.66)	13.56 (10.41, 16.53)	0.242
Plaque area (mm^2)	7.93 (6.56, 10.62)	8.19 (7.08, 10.55)	7.87 (6.21, 10.72)	0.596
PB (%)	62.5 (55.0, 68.8)	69.4 (63.5, 72.0)	60.8 (53.7, 66.5)	<0.001
TCFA phenotype	97 (66%)	19 (67.9%)	78 (65.5%)	0.816
Remodeling pattern				0.309
Constrictive remodeling	81 (55.1%)	17 (60.7%)	64 (53.8%)	
Compensatory remodeling	61 (41.5%)	9 (32.1%)	52 (43.7%)	
Excessive expansive remodeling	5 (3.4%)	2 (7.1%)	3 (2.5%)	
3D-QCA and CFD-derived variables				
3D-QCA lesion length (mm)	17.4 (13.0, 25.2)	18.3 (14.3, 25.1)	17.4 (12.4, 25.4)	0.604
MLD (mm)	2.10 (1.78, 2.52)	1.87 (1.52, 2.05)	2.23 (1.84, 2.56)	<0.001
Percentage DS (%)	25.9 (20.4, 34.0)	36.5 (24.4, 44.6)	24.9 (19.8, 30.9)	0.001
Coronary blood flow (ml/s)	0.84 (0.63, 1.17)	0.73 (0.56, 1.12)	0.88 (0.66, 1.17)	0.118
Maximum ESS value (Pa)	5.06 (3.23, 8.91)	9.40 (6.30, 12.52)	4.13 (2.99, 6.96)	<0.001
Minimum ESS value (Pa)	1.21 (0.81, 1.80)	1.17 (0.78, 0.180)	1.33 (1.03, 1.78)	0.296
Pressure drop across the lesion (mmHg)	1.95 (1.14, 3.33)	3.31 (2.28, 5.17)	1.68 (0.97, 2.67)	<0.001
Lesion location				
Coronary artery				0.212

Left anterior descending coronary artery	58 (39.5%)	13 (46.4%)	45 (37.8%)	
Left circumflex coronary artery	44 (29.9%)	11 (39.3%)	33 (27.7%)	
Right coronary artery	44 (99.9%)	4 (14.3%)	40 (33.6%)	
Intermediate coronary artery	1 (0.7%)	0 (0%)	1 (0.8%)	
Coronary segment				0.679
Proximal vessel	100 (68%)	19 (68%)	81 (68%)	
Mid vessel	27 (18%)	4 (14%)	23 (19%)	
Distal vessel	20 (14%)	5 (18%)	15 (13%)	

Table footnote: CFD, computational fluid dynamics.

Table 3. Lesion level univariable and multivariable analyses of the morphological, angiographic and hemodynamic predictors of MACE-R.

	Univariable analysis		Multivariable analysis*	
	Hazard ratio	**P**	**Hazard ratio**	**P**
Lesion length (per 1mm increase)	1.03 (1.00, 1.05)	0.030	1.00 (0.98, 1.03)	0.770
MLA (per 1mm^2 increase)	0.53 (0.38, 0.74)	<0.001	-	-
PB (per 1% increase)	1.10 (1.05, 1.16)	<0.001	1.08 (1.03, 1.14)	0.004
MLD (per 1mm increase)	0.19 (0.08, 0.44)	<0.001	-	-
Percentage DS (per 1% increase)	1.06 (1.03, 1.10)	0.001	-	-
Maximum ESS value (per 1Pa increase)	1.14 (1.08, 1.20)	<0.001	1.11 (1.05, 1.17)	0.001
Pressure drop across a lesion (per 1mmHg increase)	1.10 (1.03, 1.18)	0.005	-	-

* Significant correlation (r>0.5) was noted between the maximum ESS and the MLA (r=-0.612, P<0.001), the MLD (r=-0.586, P<0.001), the %DS (r=0.518, P<0.001) and the pressure drop across the lesion (r=-0.735, P<0.001). Maximum ESS was entered in the multivariate model as this variable had the highest area under the curve (AUC) in the receiver-operating characteristics analysis (AUC_{maxESS} = 0.790, P<0.001; AUC_{MLA} = 0.743, P<0.001; AUC_{MLD} = 0.723, P<0.001; AUC_{DS} = 0.711, P=0.001; $AUC_{pres\ drop}$ = 0.754, P<0.001).

Table 4. Lesion level univariable and multivariable analyses of the morphological, angiographic and hemodynamic predictors of MACE.

	Univariable analysis		Multivariable analysis	
	Hazard ratio	**P**	**Hazard ratio**	**P**
MLA (per 1mm^2 increase)	0.47 (0.31, 0.72)	<0.001	-	-
PB (per 1% increase)	1.11 (1.05, 1.17)	<0.001	1.09 (1.03, 1.16)	0.003
MLD (per 1mm increase)	0.20 (0.08, 0.51)	0.001	-	-
Percentage DS (per 1% increase)	1.05 (1.01, 1.09)	0.008	-	-
Maximum 3mm ESS value (per 1Pa increase)	1.15 (1.09, 1.22)	<0.001	1.12 (1.05, 1.19)	<0.001
Pressure drop across a lesion (per 1mmHg increase)	1.11 (1.03, 1.19)	0.004	-	-

* Significant correlation (r>0.5) was noted between the maximum ESS and the MLA, the MLD, the %DS and the pressure drop across the lesion. Maximum ESS was entered in the multivariate model as this variable had the highest area under the curve (AUC) in the receiver-operating characteristics analysis (AUC_{maxESS} = 0.797, P<0.001; AUC_{MLA} = 0.787, P<0.001; AUC_{MLD} = 0.737, P<0.001; AUC_{DS} = 0.688, P=0.005; $AUC_{pres\ drop}$ = 0.779, P<0.001).